

# Order to Disorder in Quasiperiodic Composites

David Morison  
nosiromdivad@gmail.com  
Department of Physics & Astronomy  
University of Utah

N. Benjamin Murphy  
murphy@math.utah.edu  
Department of Mathematics  
University of Utah

Elena Cherkaev  
elena@math.utah.edu  
Department of Mathematics  
University of Utah

Kenneth M. Golden\*  
golden@math.utah.edu  
Department of Mathematics  
University of Utah

# Order to Disorder in Quasiperiodic Composites

David Morison

*Department of Physics & Astronomy, University of Utah*

N. Benjamin Murphy, Elena Cherkaev, and Kenneth M. Golden

*Department of Mathematics, University of Utah*

Aperiodic geometries with long range order have been of scientific and engineering interest since the discovery of quasicrystals. Studies of periodic and quasiperiodic media, such as photonic crystals and quasicrystals, have largely focused on interference effects to achieve optical transport behavior analogous to electronic transport in semiconductors. Here we find similar exotic behavior in a class of Moiré-structured composites, but which is exhibited broadly by the effective electrical, magnetic, diffusive, thermal, and optical properties with *no* scattering or interference effects involved. The dependence of these bulk transport coefficients on mixture geometry is distilled into the spectral properties of an operator analogous to the Hamiltonian in quantum phenomena. As this deterministic system is tuned from periodicity to quasiperiodicity, its classical transport properties switch from those of ordered to randomly disordered materials, with spectral behavior analogous to the Anderson localization transition. Periodic media display sharp resonances, band gaps, and extended eigenstates separated by “mobility edges” of localized states, while uniformly extended eigenstates are observed in aperiodic media. Uncorrelated spectral statistics transition toward obeying the universal Wigner-Dyson distribution with level repulsion. We explore this behavior for optical materials.

## I. INTRODUCTION

In the late 1980s it was shown that in a composite patterned after a crystal, such as a dielectric material with a periodic lattice of voids, electromagnetic waves of certain frequencies and directions could be prohibited from propagating within the structure [1, 2]. This observation led to the development of photonic crystals and a theory of controlling the flow of light through structured media based on a powerful analogy that relates *photonic* band gaps to *electronic* band gaps in semiconductors, thus bringing the robust framework of solid state physics and Anderson localization to optics [1–4]. In both cases, as well as in *sonic crystals* developed to control sound propagation [5], periodicity in the composite leads to destructive interference and gaps, *e.g.*, in the Hamiltonian spectrum.

A few years prior to these developments, a metallic alloy with a quasiperiodic configuration of molecules, or *quasicrystal*, was discovered [6–8], which rewrote the foundations of crystallography. That structures with predictable long range order but no periodicity could play an important role in physics and materials science inspired a new direction in photonics research with the development of *photonic quasicrystals* [9]. Many types of these deterministic media which lack translational symmetry have been designed, studied, and used in various applications [9–13].

The discovery of quasicrystals, as well as findings on the spectrum of Hamiltonians with quasiperiodic potentials [14–16], also inspired investigation into bulk classical transport in media with quasiperiodic variations in local properties [17]. Rather than a governing wave equation, like Schrödinger’s equation, problems involving electrical conductivity  $\sigma$ , thermal conductivity  $\kappa$ , complex permittivity  $\epsilon$  in the quasistatic limit, or diffusivity  $D$  can all be formulated in terms of the same divergence form second order elliptic equation. It was found, *e.g.* in one dimension with local conductivity  $\sigma(x) = 3 + \cos x + \cos kx$ , which is periodic for  $k$  rational and quasiperiodic for  $k$  irrational, that the effective conductivity  $\sigma^*(k)$  is discontinuous in  $k$  [17], with 2D examples in [18].

Here we construct a deterministic, two-dimensional, two-phase composite – a *Moiré quasicrystal* – that enables us, along with recent advances in the theoretical analysis of composites, to study how classical transport properties behave in the transition from periodicity to aperiodicity. That is, we now have the tools to probe the physics underlying the sensitive, discontinuous dependence of bulk transport on the variations in local properties found in [17, 18]. In particular, bulk behavior is analyzed in terms of the Bergman-Milton (or Stieltjes integral) representation, which holds for the effective parameters  $\sigma^*$ ,  $\epsilon^*$ ,  $D^*$ , etc. [19–22]. It involves a spectral measure  $\mu$  of a self-adjoint operator  $G$  which depends only on the mixture geometry. In discrete settings,  $G$  becomes a real-symmetric matrix. The spectral measure  $\mu$ , local electric field  $\mathbf{E}$ , displacement  $\mathbf{D} = \epsilon\mathbf{E}$  and current  $\mathbf{J} = \sigma\mathbf{E}$  are determined by the eigenvalues and eigenvectors of  $G$ . Through this spectral distillation and recent results on computing  $\mu$  [23] and analyzing its behavior through the lens of random matrix theory [24], we can now formulate and examine classical transport in composites, and quasiperiodic media in particular, in terms of the theory of localization and band gaps in solid state physics, as was done for photonic crystals and quasicrystals in the scattering regime.

We find that as the geometry is tuned from periodic to quasiperiodic, the eigenvalues, eigenmodes, profile of  $\epsilon^*$ , and localization properties of  $\mathbf{E}$  undergo an order-to-disorder transition analogous to the Anderson transition.

54 Spectral measures for periodic systems have sharp resonances that induce dramatic variability in band and absorption  
 55 characteristics, and in profiles of  $\epsilon^*$ . Regions of extended eigenstates are separated by “mobility edges” of localized  
 56 states, and  $\mathbf{E}$  is localized for certain frequencies and extended for others. As the geometry is tuned to aperiodicity, the  
 57 behavior of  $\mu$  and  $\epsilon^*$  resembles that of the 2D random percolation model at its threshold, with extended eigenstates,  
 58 pronounced spectral endpoint behavior, and Wigner-Dyson eigenvalue statistics with strong level repulsion [24].

59 The spectral characteristics considered here govern the optical characteristics of nanostructured bimetallic films  
 60 [25, 26] and depositions of nanosized metal particles on thin dielectric substrates [27–30], which change as a function  
 61 of heterogeneous surface structure composition and geometry. This enables tunability of their optical responses for  
 62 nano-plasmonic device applications [25–30]. The long wavelength quasistatic assumption holds in the visible range  
 63 [31], and these systems are described macroscopically by the Stieltjes integral representations for  $\epsilon^*$  or  $\sigma^*$ . Resonances  
 64 in  $\mu$  explain giant surface-enhanced Raman scattering observed in semicontinuous films [26, 32, 33], and induce strong  
 65 fluctuations in  $\mathbf{E}$  and the dielectric profile of  $\epsilon^*$ , associated with the excitation of collective electronic surface plasmon  
 66 modes [31]. We numerically explore these phenomena in 2D impedance networks with quasiperiodic microgeometry  
 67 and discuss our results using random matrix theory.

68

## II. METHODS

69 Homogenized coefficients for macroscopic two-phase composite materials, including electrical and thermal conductivity,  
 70 diffusivity, complex permittivity, and magnetic permeability, can all be defined in terms of the same elliptic  
 71 partial differential equation [22]. For complex permittivity in the quasistatic regime, such as the metal-dielectric  
 72 mixtures in visible light discussed above, the system is described locally by

$$\nabla \cdot (\epsilon \nabla \phi) = 0, \quad (1)$$

73 with potential  $\phi$ , electric  $\mathbf{E} = -\nabla \phi$  and displacement  $\mathbf{D} = \epsilon \mathbf{E}$  fields, and local complex permittivity  $\epsilon$  taking frequency  
 74 dependent values  $\epsilon_1(\omega)$  or  $\epsilon_2(\omega)$ . The fields  $\mathbf{E}$  and  $\mathbf{D}$  satisfy  $\nabla \times \mathbf{E} = 0$  and  $\nabla \cdot \mathbf{D} = 0$ , with  $\epsilon = \epsilon_1 \chi_1 + \epsilon_2 \chi_2$ , where  
 75  $\chi_1 = 1$  in medium 1 and is zero otherwise, with  $\chi_2 = 1 - \chi_1$ .

76 The effective permittivity matrix  $\epsilon^*$  can be defined by  $\langle \mathbf{D} \rangle = \epsilon^* \langle \mathbf{E} \rangle$  with  $\langle \mathbf{E} \rangle = \mathbf{E}_0$ , where  $\langle \cdot \rangle$  denotes spatial average  
 77 and  $\mathbf{E}_0 = E_0 \mathbf{e}_k$  for some standard basis vector  $\mathbf{e}_k$ ,  $k = 1, \dots, d$ , where  $d$  is dimension. Equivalently, it can be defined  
 78 in terms of the system energy  $\langle \mathbf{D} \cdot \mathbf{E} \rangle = \epsilon_{kk}^* E_0^2$ , where  $\epsilon_{kk}^*$  is the  $k$ th diagonal coefficient of the matrix  $\epsilon^*$ , which we  
 79 denote by  $\epsilon^* = \epsilon_{kk}^*$ . The key step in the analytic continuation method [19–23] is the Stieltjes integral representation  
 80 for  $\epsilon^*$ ,

$$F(s) = 1 - \frac{\epsilon^*}{\epsilon_2} = \int_0^1 \frac{d\mu(\lambda)}{s - \lambda}, \quad s = \frac{1}{1 - \epsilon_1/\epsilon_2}. \quad (2)$$

81 Here,  $F(s) = \langle \chi_1 \mathbf{E} \cdot \mathbf{E}_0 \rangle / (s E_0^2)$  and  $-F(s)$  plays the role of an effective electric susceptibility. Thus, the method  
 82 defines a homogeneous medium immersed in a uniform field  $\mathbf{E}_0$  that behaves macroscopically and energetically the  
 83 same as the inhomogeneous composite medium.

84 Equation (2) follows from the resolvent for  $\mathbf{E}$  [21, 23]

$$\chi_1 \mathbf{E} = s(sI - G)^{-1} \chi_1 \mathbf{E}_0, \quad G = \chi_1 \Gamma \chi_1, \quad (3)$$

85 where  $\mu$  is a spectral measure of the operator  $G$  and  $\Gamma = -\nabla(-\Delta)^{-1} \nabla \cdot$  is the projection onto curl-free fields, based  
 86 on convolution with the Green’s function for the Laplacian  $\Delta = \nabla^2$ . A key feature of equations (2) and (3) is that  
 87 the material parameters in  $s$  and the applied field strength  $E_0$  are *separated* from the geometric complexity of the  
 88 system, which is encoded in the properties of the spectral measure  $\mu$  and its moments  $\mu_n = \int_0^1 \lambda^n d\mu(\lambda)$ . For example,  
 89  $\mu_0 = \langle \chi_1 \rangle = p$ , the volume fraction (or area fraction) of medium 1. All of the effective coefficients of the composite  
 90 material mentioned above are represented by Stieltjes integrals with *the same*  $\mu$  [34].

91 While the measure  $\mu$  can include discrete and/or continuous components [22], it reduces to a weighted sum of Dirac  
 92  $\delta$ -functions  $\delta(\lambda - \lambda_j)$  for media such as laminates, hierarchical coated cylinder and sphere assemblages, and finite *RLC*  
 93 impedance networks [22, 23]. Here, we investigate effective transport properties of square two-component impedance  
 94 networks of size  $L$  and periodic and quasiperiodic 2D microgeometry, via the dielectric profile of  $\epsilon^*$ , localization  
 95 and intensity of  $\mathbf{E}$  and  $\mathbf{D}$ , and spectral properties of  $\mu$ . In this setting,  $G = \chi_1 \Gamma \chi_1$  is a real-symmetric matrix of  
 96 size  $N = 2L^2$ ,  $\chi_1$  is a diagonal matrix with 1’s and 0’s along the diagonal corresponding to bond type, and  $\Gamma$  is a  
 97 projection matrix. The measure  $\mu$  is determined by the eigenvalues  $\lambda_j$  and eigenvectors  $\mathbf{v}_j$  of  $N_1 \times N_1$  submatrices of  
 98  $\Gamma$  corresponding to diagonal components  $[\chi_1]_{jj} = 1$ , with

$$d\mu(\lambda) = \sum_j m_j \delta(\lambda - \lambda_j) d\lambda, \quad m_j = (\mathbf{v}_j \cdot \chi_1 \hat{\mathbf{e}}_k)^2, \quad (4)$$

<sup>99</sup>  $j = 1, \dots, N_1$ ,  $N_1 \approx pN$  (total number of  $\epsilon_1$  bonds), and  $\hat{\mathbf{e}}_k$  is a standard basis vector on the lattice [24]. In this case,  
<sup>100</sup> equations (2) and (3) become finite sums with [23]

$$F(s) = \sum_j \frac{(\mathbf{v}_j \cdot \chi_1 \hat{\mathbf{e}}_k)^2}{s - \lambda_j}, \quad \chi_1 \mathbf{E} = s E_0 \sum_j \frac{(\mathbf{v}_j \cdot \chi_1 \hat{\mathbf{e}}_k)}{s - \lambda_j} \mathbf{v}_j. \quad (5)$$

<sup>101</sup> We now introduce a Moiré-type class of 2D two-component composites that are tunable to be periodic or aperiodic  
<sup>102</sup> as follows. Consider a square lattice with standard basis vectors  $\mathbf{e}_1$  and  $\mathbf{e}_2$ , bond midpoints  $(x, y) \in \mathbb{R}^2$ , and the  
<sup>103</sup> scaled rotation transformation  $T$  given by

$$T : (x, y) \mapsto (a, b), \quad T = r \begin{pmatrix} \cos \theta & -\sin \theta \\ \sin \theta & \cos \theta \end{pmatrix}. \quad (6)$$

<sup>104</sup> Now consider the function  $\psi(a, b) = \cos(2\pi a) \cos(2\pi b)$ . The geometry of the two material phases is determined by the  
<sup>105</sup> condition:  $\chi(x, y) = 1$  for all  $(x, y) \in \mathbb{R}^2$  such that  $\psi(T(x, y)) \geq \psi_0$  and zero otherwise. We focus on the value  $\psi_0 = 0$   
<sup>106</sup> which generates composite microstructure with a fraction  $p \approx 1/2$  of type one bonds. We do so to compare features of  
<sup>107</sup> deterministically tuned quasiperiodic systems to that of the random percolation model near the percolation transition  
<sup>108</sup>  $p = p_c = 1/2$  [35, 36].

<sup>109</sup> Primitive translation vectors for  $\psi$  are  $\mathbf{t}_1 = (1/2, 1/2)$  and  $\mathbf{t}_2 = (1/2, -1/2)$ . When  $r$  and  $\theta$  are chosen such that  
<sup>110</sup>  $T : (m\mathbf{e}_1 + n\mathbf{e}_2) \mapsto (m'\mathbf{t}_1 + n'\mathbf{t}_2)$  for integer values of  $m, n, m'$  and  $n'$ , then  $\chi$  has finite period  $K = \sqrt{m^2 + n^2}$ , and  
<sup>111</sup> has infinite period otherwise. The arrangement of  $r$  and  $\theta$  such that  $K < \infty$  is fractal in nature, as shown in Figure  
<sup>112</sup> 1. The arrangement of finite periods  $(r, \theta)$  is similar to fractals defined in terms of rational numbers on the real line,  
<sup>113</sup> such as Thomae's function.

### III. RESULTS

<sup>114</sup> The Moiré system introduced above is parameterized by  $r > 0$  and  $0 \leq \theta < 2\pi$ , which generates a diverse  
<sup>115</sup> assortment of periodic ("finite period") and quasiperiodic ("infinite period") microgeometries. To numerically calculate  
<sup>116</sup> mathematical and physical quantities, we consider finite subsets of these systems as *RLC* impedance networks. The  
<sup>117</sup> examples displayed in Figure 2a hint at the geometric richness of this composite class. The bond color indicates the  
<sup>118</sup> modulus value of  $\mathbf{E}$  in phase 1, i.e.,  $|\chi_1 \mathbf{E}|$ , calculated via (5). Since  $\chi_1 \mathbf{D} = \epsilon_1 \chi_1 \mathbf{E}$  these colors also specify displacement

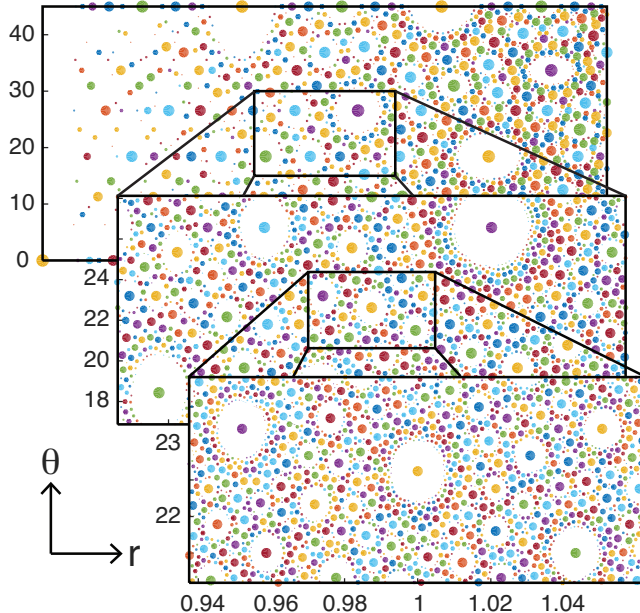
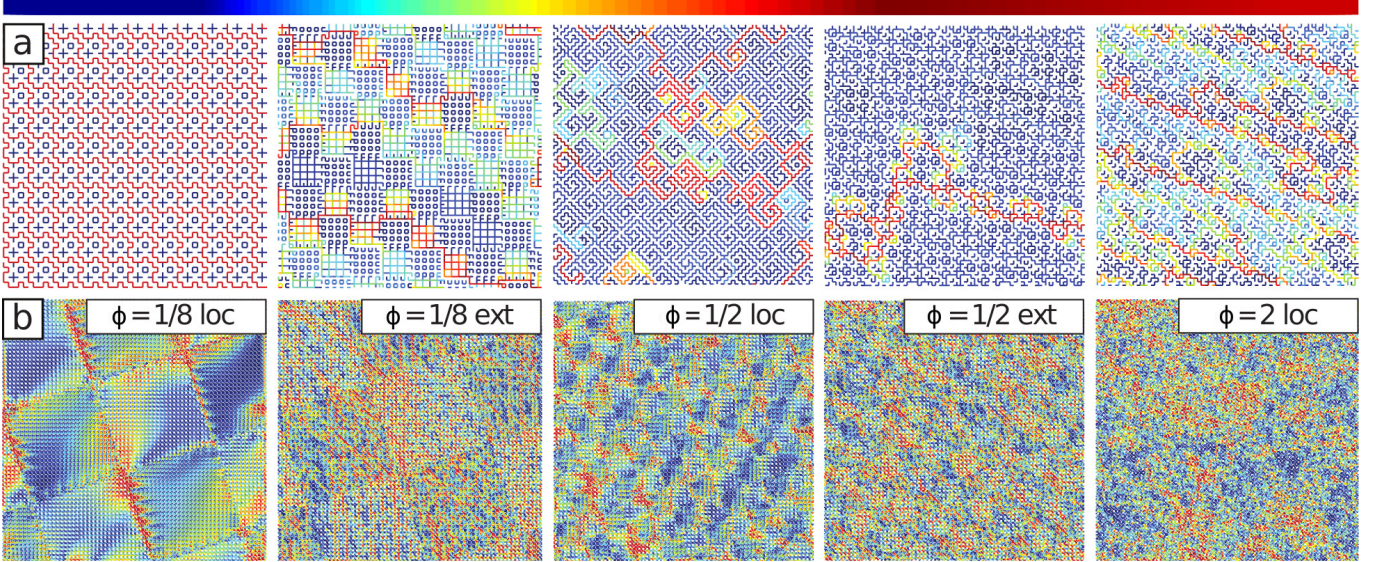


FIG. 1. **Fractal arrangement of periodic systems.** Sequential insets zooming into smaller regions of parameter space. Dots identify  $(r, \theta)$  values corresponding to systems with periodic microgeometries, where short and large periods are identified by large and small dots, respectively, revealing self similar, fractal arrangements of periodic systems.



**FIG. 2. Quasiperiodic composite microgeometry and Anderson localization of fields.** Moiré interference patterns generated by the transformation (6) give rise to a large class of composite materials with periodic and quasiperiodic microgeometry. Subsections of such media are shown with small square system sizes 53, 73, 73, 73, and 73 from left to right in (a) to display detail and larger system size 199 in (b). Cool and warm colors correspond to near-zero and large values of  $|\chi_1\mathbf{E}|$  or  $|\chi_1\mathbf{D}|$ , respectively, with color bar at the top showing the saturated linear scale. (a) An assortment of composites displaying the large microgeometry variability of the class. (b) Anderson localization of fields in quasiperiodic media. For small values of  $\phi$ , fields exhibit a frequency dependent transition from localized (loc) to extended (ext). The localization phenomenon diminishes as  $\phi \rightarrow 2$  and fields are qualitatively similar for all frequencies away from  $\omega = 0$  and resemble the rightmost panel in (b) and that of the percolation model near the percolation threshold  $p = p_c$ .

values, with a change in scale by  $|\epsilon_1|$ . In this section, we investigate a small swath of the large parameter space, for  $r = 10/\sqrt{3}$  and  $\arctan(1/3) \leq \theta \leq \arctan(1/3) + \phi$  for  $0 \leq \phi \leq 2$  (degrees), starting from a short period system. Figures 2b and 3a display examples of this region of parameter space and show that such a small change in the Moiré twist angle  $\theta$  gives rise to a dramatic transition in composite microgeometry — from a short period system with orderly field (or current) paths to quasiperiodic systems with disorderly, meandering paths similar to those exhibited by the random percolation model near  $p = p_c$ .

When the fields are plotted *vs.*  $s$ ,  $0 \leq \text{Re } s \leq 1$  (equivalently, *vs.* frequency  $\omega$ ) with  $\text{Im } s \ll 1$  a frequency dependent localization/delocalization transition of fields is revealed for small values of  $\phi \in [0, 2]$ , as shown in Figure 2b for  $\phi = 1/8$  and  $1/2$ . In contrast, the fields for angles closer to  $\phi = 2$  are more disordered and resemble those in the random percolation model, and are qualitatively similar to the rightmost panel in Figure 2b for all  $0 \leq \text{Re } s \leq 1$ . We investigate these and other phenomena through mathematical and physical quantities such as the spectral measure  $\mu$ , correlations of its eigenvalues, localization of its eigenvectors, dielectric profiles of  $\epsilon^*$ , localization of  $\mathbf{E}$ , etc.

A large variety of physical phenomena exhibited by inhomogeneous materials can be described by two component *RLC* impedance networks [32]. Each of the two components is created by combining a resistor  $R$ , inductor  $L$ , and capacitor  $C$  in a way that achieves an impedance characteristic of the material being modeled. For example, a Drude-metal/dielectric composite is modeled by  $R$  and  $L$  in series, in parallel with  $C$  for one component, and  $C$  for the other [31], yielding a plasma frequency  $\omega_p^2 = 1/LC$  and relaxation time  $\tau = L/R$ . As Kirchhoff's network laws are discrete versions of the curl-free and divergence-free conditions on the fields in equation (1), these *RLC* impedance networks really do resemble the continuum composites they are intended to model [31].

Indeed, the AC response and polarization effects observed in a variety of conductor-dielectric mixtures at low frequencies are described by an *R-C* model [32, 33]. While metal-dielectric composites exhibiting collective electronic modes at higher, optical frequencies such as (surface) plasmon resonances are described by an *RL-C* model [32, 33]. The dependence of  $s(\omega)$  on frequency  $\omega$  is model specific. For the *R-C* and *RL-C* models,  $0 \leq \text{Re } s < 1$  for  $0 \leq \omega < \infty$  and  $\delta \leq \text{Im } s < 0$ , where  $|\delta|$  can be chosen as small as desired by increasing the quality factor  $Q$ , with  $\text{Re } s \rightarrow 1$  and  $\text{Im } s \rightarrow 0$  as  $\omega$  increases [32, 33]. In order to give a model independent description of the phenomena investigated here, we plot  $s$ -dependent quantities using  $0 \leq \text{Re } s \leq 1$  and  $\text{Im } s = 0.001$  fixed.

The frequency dependence of the spectral measure  $\mu$ , its eigenvalues, and localization properties of its eigenvectors, shown in Figure 3, govern the frequency dependence of the dielectric profile of  $\epsilon^*$  and the localization properties of

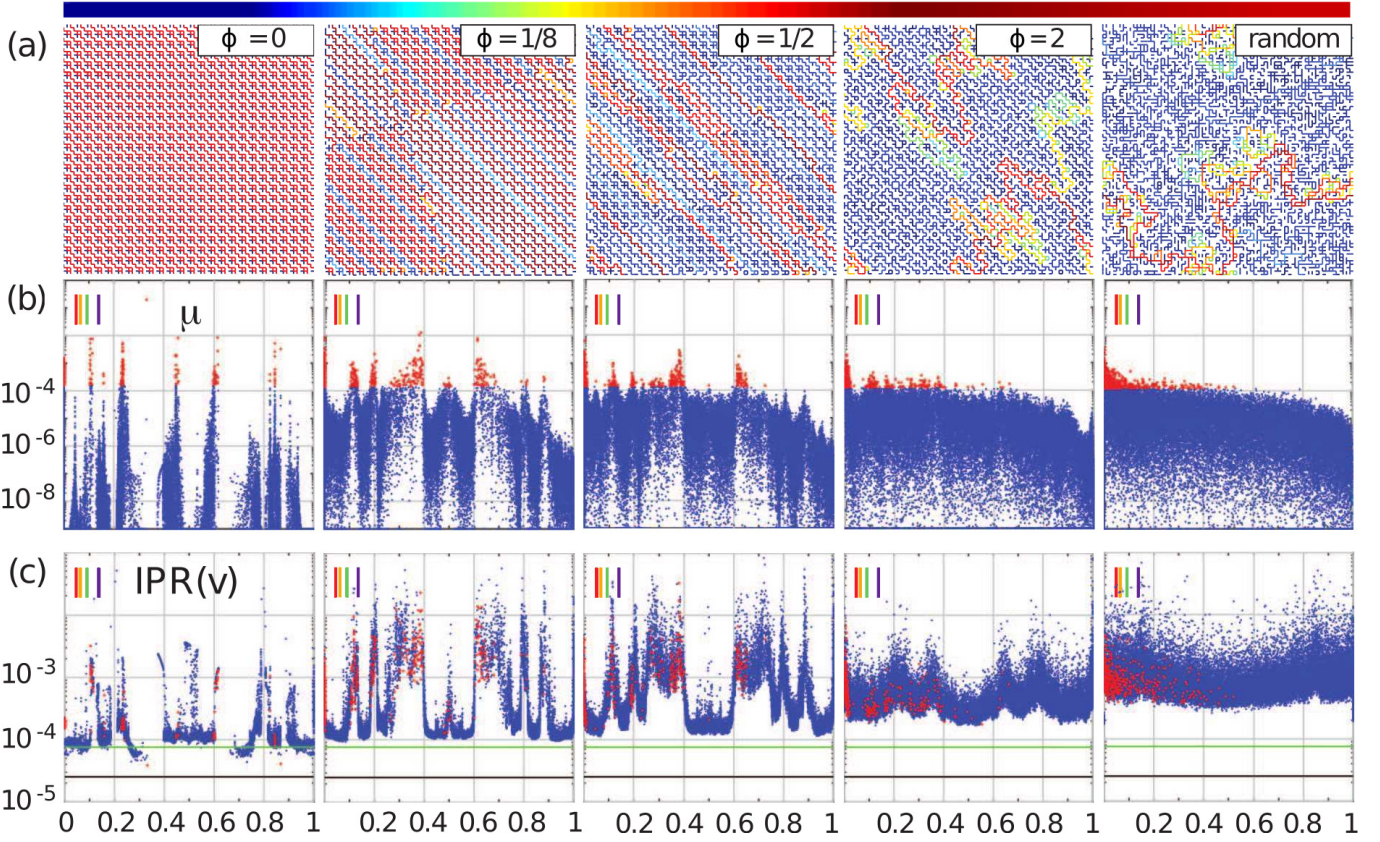


**FIG. 3. Frequency dependence of the spectral measure and eigenvector localization.** Composite microgeometry and fields, spectral measure  $\mu$ , and eigenvector  $IPR$  plotted for various values of the Moiré twist angle  $\theta$ , with  $0 \leq \phi \leq 2$  and square system size 73 in (a) to show detail and 199 in (b) and (c). (a) Composite microgeometry and fields. Cool and warm colors correspond to near-zero and large values of  $|\chi_1 \mathbf{E}|$  or  $|\chi_1 \mathbf{D}|$ , respectively, with color bar at the top showing the saturated linear scale. (b) Masses  $m_j$  of  $\mu$  plotted *vs.* eigenvalues  $0 \leq \lambda_j \leq 1$  of the matrix  $G$  (equivalently frequency). Red dots indicate the largest masses, used as indicators in (c) below. (c)  $IPR$  values for the eigenvectors  $\mathbf{v}_j$  of  $G$ ,  $IPR(\mathbf{v})$ , plotted *vs.*  $\lambda_j$ . Green and black horizontal lines indicate  $IPR$  values for GOE and completely extended vectors,  $3/N_1$  and  $1/N_1$ , respectively. The short period system with  $\phi = 0$  and those with small  $\phi$  are characterized by sharp resonances in  $\mu$ . The largest spectral masses  $m_j$  of  $\mu$  are either associated with extended  $\mathbf{v}_j$  with  $IPR$  values near or below the GOE value, or are associated with “mobility edges” with large  $IPR$  variability. As  $\phi \rightarrow 2$ , the dramatic variation in these quantities diminishes and begins to resemble that of the random percolation model at the percolation transition,  $p = p_c = 1/2$ , shown in the rightmost panels.

the fields shown in Figure 4. For the short period system with  $\phi = 0$  shown in Figure 3a, the spectral measure  $\mu$  in Figure 3b is comprised of sharply peaked resonances, which are due to the largest measure masses  $m_j$  (shown in red) and/or a large density of eigenvalues  $\lambda_j$ , which are singularities of  $\epsilon^*$  for  $Im s = 0$ . As  $\phi$  increases and the composite microgeometry becomes quasiperiodic, the resonant peaks of  $\mu$  away from  $\omega = 0$  spread out, change frequency locations, and diminish in strength. As  $\phi \rightarrow 2$ , the resonances in  $\mu$  continue to spread out until all but the Drude resonance diminish, and  $\mu$  and  $\epsilon^*$  begin to resemble those of the random percolation model for  $p = p_c$ .

The singularities in  $\mu$  have a physical interpretation in terms of relaxation times in the transient response in the *R-C* model, or in terms of dielectric resonances in the *RL-C* model [32, 33]. The dielectric resonances observed for the *RL-C* model with percolative geometry have been argued to provide a natural explanation for the anomalous fluctuations of the local electric field  $\mathbf{E}$ , which are responsible for giant surface-enhanced Raman scattering observed, for example, in semicontinuous metal films [33]. We show below that resonances in  $\mu$  for periodic and quasiperiodic media indeed give rise to dramatic fluctuations in  $\epsilon^*$ ,  $\mathbf{E}$ , and  $\mathbf{D}$ .

Figure 3c displays the inverse participation ratio ( $IPR$ ) for the eigenvectors  $\mathbf{v}_j$ ,  $j = 1, \dots, N_1$ , of  $G$  for various values of  $\phi$ , as a function of the eigenvalues  $\lambda_j$ . The  $IPR$  characterizes *localization* phenomenon: for a unit vector  $\mathbf{u}$ ,  $IPR(\mathbf{u}) = 1$  for a completely localized vector with only one non-zero component and  $IPR(\mathbf{u}) = 1/N_1$  for a completely extended vector  $\mathbf{u} \in \mathbb{R}^{N_1}$  with all components equal in value [24]. For Gaussian orthogonal ensemble (GOE) matrices, the eigenvectors are quite extended with a mean asymptotic  $IPR$  value of  $3/N_1$  [24]. The  $1/N_1$  and  $3/N_1$  values are shown in Figure 3c as black and green lines for reference.

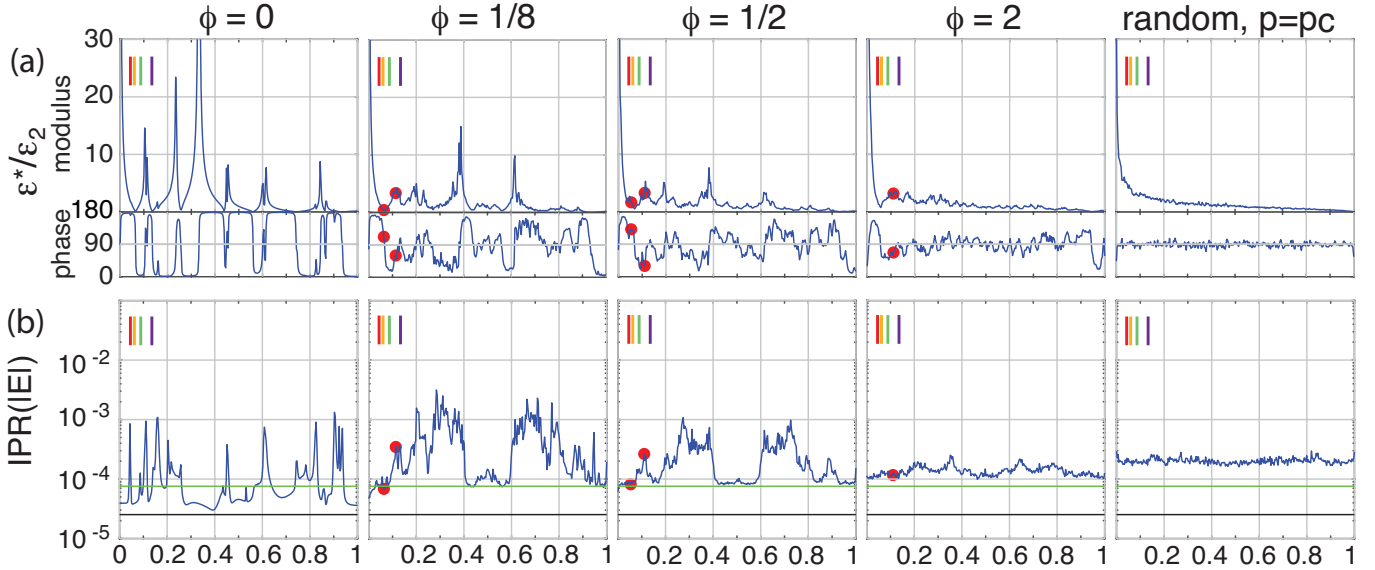


**FIG. 4. Frequency dependence of dielectric profile and field localization.** Normalized effective complex permittivity  $\epsilon^*/\epsilon_2$  and  $IPR$  of the point-wise modulus of the electric field  $\chi_1\mathbf{E}$ , normalized to unity,  $IPR(\mathbf{E})$ , plotted for various values of the Moiré twist angle  $\theta$ , with  $0 \leq \phi \leq 2$ , versus  $0 \leq \text{Re } s \leq 1$  (equivalently frequency) and  $\text{Im } s = 0.001$ . (a) Amplitude and phase of  $\epsilon^*/\epsilon_2$  plotted versus  $\text{Re } s$ . The color bars in the upper left of the panels are for reference and indicate the optical range for impedances corresponding to the Drude model for a gold/vacuum composite. (b)  $IPR(\mathbf{E})$  or equivalently  $IPR(\mathbf{D})$  plotted vs.  $\text{Re } s$ . The short period system with  $\phi = 0$  and those with small  $\phi$  are characterized by dramatically fluctuating dielectric profiles in  $\epsilon^*$ , due to sharp resonances in  $\mu$ . The variability in the eigenvector  $IPR$  in Figure 3c induces dramatic variability and mobility edges in  $IPR(\mathbf{E})$  and  $IPR(\mathbf{D})$ . As  $\phi \rightarrow 2$ , their variations diminish and begin to resemble those of the random percolation model at its threshold,  $p = p_c = 1/2$ , shown in the rightmost panels. Red dots indicate values of  $\text{Re } s$  used in Figure 2b: for  $\phi = 1/8$ ,  $\text{Re } s = 0.063, 0.115$ , for  $\phi = 1/2$ ,  $\text{Re } s = 0.055, 0.111$ , and for  $\phi = 2$ ,  $\text{Re } s = 0.111$ .

For the short period system with  $\phi = 0$ , Figures 3b and 3c show that frequencies where the masses  $m_j$  of  $\mu$  are largest (shown in red) correspond either to very extended eigenvectors or "mobility edges" where the values  $IPR(\mathbf{v}_j)$  have dramatic variability for small changes in  $\lambda_j$ . For the latter, the eigenvector expansion of  $\chi_1\mathbf{E}$  in equation (5) indicates these resonant frequencies of  $\mu$  correspond to large variability in both the field strength and field localization, for small frequency changes when  $\text{Im } s \ll 1$  (equivalently for displacement  $\chi_1\mathbf{D}$ ), as in the leftmost panel of Figure 2b. We will make this correspondence more precise below.

Figure 4a displays  $\epsilon^*/\epsilon_2$  for various values of the Moiré twist angle  $\theta$ , with  $0 \leq \phi \leq 2$ , as a function of  $\text{Re } s$  (equivalently frequency  $\omega$ ). Color bars are included in the upper left of the panels that indicate the optical range for impedances corresponding to the Drude model of a gold/vacuum composite. The Drude peak at  $\omega = 0$  ( $s = 0$ ) present for all values of  $\phi$  indicates the composite is conducting for  $\omega = 0$  [31]. For the short period system with  $\phi = 0$ , there are several values of  $\omega$  where  $|\epsilon^*|$  is sharply peaked (and diverges as  $\text{Im } s \rightarrow 0$ ). These frequencies correspond to the so-called surface plasmon resonance, which characteristically shows up as a strong absorption line in experiments [31].

For  $\phi = 0$ , the frequencies where the resonances of  $\mu$  are strongest are precisely where  $|\epsilon^*|$  is sharply peaked, and also where  $\epsilon^*$  undergoes a dramatic switch in phase. This switch in phase gives rise to an "optical transition," where  $\epsilon^*$  changes from inductive to capacitive — a phenomenon observed in optical cermets [32]. These phase switches also occur at the troughs of  $|\epsilon^*|$ , where  $\mu$  has very small mass. The correspondence of optical transition frequencies with the peaks and troughs of  $|\epsilon^*|$  is due to simple analytic properties of the integral representation for  $\epsilon^*$  in (2), or sum in (5) [22]. As  $\phi$  increases, the optical transition frequencies still correspond to the peaks and troughs in  $|\epsilon^*|$ , though the frequency dependence of these features becomes more complex.

The  $IPR$  for  $|\chi_1\mathbf{E}|$  (normalized to unit length) provides a measurement of localization for the electric field itself – equivalently for the normalized displacement field  $\chi_1\mathbf{D} = \epsilon_1\chi_1\mathbf{E}$ . Figures 3c and 4b show there is a close relationship between the eigenvector  $IPR$ ,  $IPR(\mathbf{v})$ , plotted vs.  $\lambda_j$  and the electric field  $IPR$ ,  $IPR(\mathbf{E})$ , plotted vs.  $\text{Re } s$ , as anticipated above. Specifically, there are frequency regions where the eigenmodes and the electric field are simultaneously localized or extended. Moreover, for  $\phi = 0, 1/8$ , and  $1/2$  there are several clear mobility edges in  $IPR(\mathbf{E})$ , following those in  $IPR(\mathbf{v})$ , showing high variability in field localization for small changes in  $\omega$ , which also correspond to resonant frequencies of  $\mu$  and high variability in field intensity. This and the relationship between  $\mu$  and  $\epsilon^*$  discussed above, indicate a high degree of *tunability* in the frequency dependent dielectric profile and electric field localization

and intensity for these values of  $\phi$ . Moreover, the microstructure is tunable via the scale  $r$  and Moiré twist angle  $\theta$  — which can be controlled by fabrication methods, such as those discussed in [37], where a small change in Moiré twist angle for bilayer graphene induces a change in conductivity similar to what we observe here for  $\epsilon^*$ . This tunability makes our Moiré-type composite class an ideal test bed for potential engineering applications.

In Figure 2b the localized (loc) and extended (ext) fields for  $\phi = 1/8, 1/2$ , and 2 were computed for values of  $\text{Re } s(\omega)$  with optical frequencies  $\omega$  — indicated by red dots in Figure 4. Comparing these two figures for the panels with values  $\phi = 1/8$  and  $1/2$ , shows *for the same microstructure*, there is a tunable localization/delocalization transition in the displacement field and associated transition in the dielectric profile for  $\epsilon^*$ . Moreover, the panels for localized (loc) fields in Figure 2b also correspond to resonant peaks in  $\mu$  in Figure 3b, which accounts for the high variability in the field intensity in Figure 2b. Furthermore, Figure 4 for  $\phi = 1/8$  and  $1/2$ , show that toward the infrared end of the spectrum the displacement field is extended and  $\epsilon^*$  is inductive, while toward the ultraviolet end of the spectrum the displacement field is more localized and  $\epsilon^*$  is capacitive. However, as  $\phi$  surpasses  $1/8$ , the larger checkerboard scale for  $|\chi_1 \mathbf{E}|$  shown in Figure 2b decreases in size until  $|\chi_1 \mathbf{E}|$  qualitatively resembles that of the percolation model for  $p = p_c$  as  $\phi \rightarrow 2$ , with more uniformly extended fields qualitatively the same for all  $0 < \text{Re } s \leq 1$  away from the Drude peak at  $\omega = 0$ , as shown in the far right panel for Figure 2b and the two rightmost panels of Figure 3a.

In Figure 4b for  $\phi = 1/8, 1/2$ , it is shown that frequency values associated with  $\text{Re } s \approx 0.4, 0.6$  (far outside the optical range) correspond to especially well-defined "mobility edges" aligned with resonant peaks in  $\mu$ , followed by large decreases in measure mass. These induce significant variations in localization and intensity of  $\mathbf{E}$  and  $\mathbf{D}$ , and dielectric profile for quite small changes in frequency, which diminish with increasing  $\phi$ .

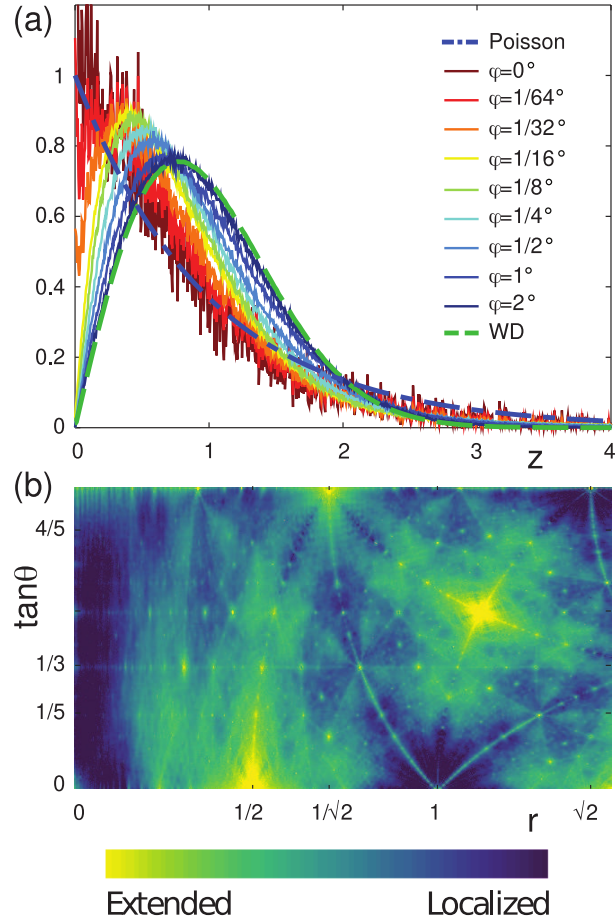
Statistical quantities for the eigenvalues  $\lambda_j$  of  $\mu$  provide insights into why the high density resonances of  $\mu$ , present for the short period system with  $\phi = 0$ , spread out as  $\phi$  increases and the composite microgeometry becomes quasiperiodic. The nearest neighbor eigenvalue spacing distribution (ESD)  $P(z)$  was initially introduced in random matrix theory by Dyson and Mehta to describe fluctuations of characteristic quantities for random systems, but has since accurately described quantities for non-random systems with sufficient complexity [38]. The ESD probes short range correlations of eigenvalues [38]. For highly correlated Wigner-Dyson (WD) spectra exhibited by, for example, the Gaussian orthogonal ensemble (GOE) of real-symmetric random matrices, the ESD is accurately approximated by  $P(z) \approx (\pi z/2) \exp(-\pi z^2/2)$ , Wigner's surmise, which illustrates *eigenvalue repulsion*, vanishing linearly as spacings  $z \rightarrow 0$  [38, 39]. In contrast, the ESD for uncorrelated Poisson spectra,  $P(z) = \exp(-z)$ , allows for significant level degeneracy [38].

Figure 5a displays the ESD for the eigenvalues  $\lambda_j$  of  $G$  for several values of  $0 \leq \phi \leq 2$ . The blue dash-dot curve is the ESD for Poisson spectra, while the green dashed curve is the ESD for the GOE. For  $\phi = 0, 1/64$ , and  $1/32$ , the sharply peaked resonances in  $\mu$  with high eigenvalue density give rise to a significant probability of zero spacings, with  $P(0) \gtrsim 0.4$ . However, as  $\phi$  increases and the composite microgeometry becomes quasiperiodic, the behavior of the ESDs starts to be characterized by weakly correlated Poisson-like statistics [39], also observed for eigenvalues of  $G$  for the low volume fraction percolation model [24]. They increase linearly from zero but the initial slope of  $P(z)$  is steeper than in the WD case, implying less repulsion. As  $\phi \rightarrow 2$ , the slope of  $P(z)$  decreases, indicating an increase in level repulsion, causing the eigenvalues of  $\mu$  to spread out as the ESD transitions toward obeying that of the GOE, characterized by highly correlated eigenvalues with strong level repulsion.

We conclude this section with a discussion of Figure 5b, which displays the average eigenvector *IPR* with yellow hues corresponding to highly extended eigenmodes — hence displacement fields — associated with short period systems, and dark green to blue hues corresponding to quasiperiodic systems with more uniformly extended eigenmodes. A single snapshot, revealing the great diversity of this class of composite materials with myriad microgeometric variations, each with a potentially distinct frequency dependence in both the field localization/delocalization characteristics and dielectric profile for  $\epsilon^*$ . Figure 1 shows that the arrangement of finite period systems is fractal in nature. It is clear from Figures 5b and 1 that we have merely scratched the surface in describing this fascinating class of composite materials with tuneable capabilities in both frequency and geometry, potentially enabling materials to be fabricated that achieve desired field characteristics and dielectric responses suitable for a broad range of engineering applications.

#### IV. CONCLUSION

Bulk electromagnetic transport properties of a Moiré-type class of 2D composite materials is explored using a Stieltjes integral integral representation for the effective complex permittivity  $\epsilon^*$ , involving a spectral measure  $\mu$  of a real-symmetric matrix  $G$ , and a summation formula for the displacement field  $\mathbf{D}$ , involving the eigenvalues  $\lambda_i$  and eigenvectors  $\mathbf{v}_i$  of  $G$ . The localization properties of  $\mathbf{D}$  and the dielectric profile for  $\epsilon^*$  are analyzed as the Moiré twist angle  $\theta$  varies 2 degrees. This small change in  $\theta$  gives rise to a sharp transition in the microgeometry of the composite material, from periodic to quasiperiodic as the period increases *ad infinitum*. Short period systems are characterized by sharp resonances in  $\mu$  which gives rise to optical frequencies  $\omega$  where  $\epsilon^*$  is sharply peaked (so-



**FIG. 5. Eigenvalue spacings and eigenvector localization.** (a) The eigenvalue spacing distribution (ESD)  $P(z)$  for various values of (Moiré) twist angle  $\theta$ , with  $0 \leq \phi \leq 2$ . The short period system for  $\phi = 0$  and those with small twist angles  $0 \leq \phi \leq 1/32$  are characterized by spectral measures  $\mu$  with very sharp resonances leading to  $P(0) \gtrsim 0.4$ . However, for  $\phi \geq 1/16$  the system begins to transition towards WD statistics with level repulsion, so that  $P(0) = 0$ . Level repulsion increases with increasing  $\phi$  as the ESD approaches the WD ESD, characterized by strong correlations and strong eigenvalue repulsion. (b) Average eigenvector  $IPR$  plotted vs.  $(r, \tan\theta)$ . Yellow hues correspond to systems with highly extended eigenmodes (hence extended electric and displacement fields) and “mobility edges” with large localization variability associated with short period systems. Dark green to blue hues correspond to quasiperiodic systems with more uniformly extended eigenmodes. This panel indicates periodic systems have a repeating pattern that turns out to be fractal in nature, as indicated in Figure 1.

248 called surface plasmon resonance frequencies) and  $\epsilon^*$  undergoes an “optical transition” from inductive to capacitive.  
 249 Moreover,  $\mathbf{D}$  is highly extended for certain ranges of frequency, separated by small “mobility edge” frequency regions  
 250 of large localization variability, that follow the resonant peaks of  $\mu$ , where  $\mathbf{D}$  is localized. These characteristics make  
 251 the dielectric profile and field response highly tunable, a desired feature in engineering applications. As the system  
 252 is tuned to quasiperiodicity, an increase in eigenvalue repulsion, as measured by the eigenvalue spacing distribution  
 253 (ESD), causes the sharp resonances of  $\mu$  to spread out, while the localization characteristics of  $\mathbf{D}$  and the dielectric  
 254 profile of  $\epsilon^*$  begin to qualitatively resemble those of the percolation model near its transition point.

255 **Acknowledgements.** We gratefully acknowledge support from the Division of Mathematical Sciences at the U.S.  
 256 National Science Foundation through Grant DMS-1715680 and the Office of Naval Research Applied and Compu-  
 257 tational Analysis Program through Grant N00014-18-1-2552. We also thank Valy Vardeny and Sarah Li for helpful  
 258 conversations.

- [1] Yablonovitch, E. Inhibited spontaneous emission in solid-state physics and electronics. *Phys. Rev. Lett.* **58**, 2059–2062 (1987).
- [2] Yablonovitch, E. & Gmitter, T. J. Photonic band structure: the face-centered-cubic case. *Phys. Rev. Lett.* **63**, 1950–1953 (1989).
- [3] John, S. Strong localization of photons in certain disordered dielectric superlattices. *Phys. Rev. Lett.* **58**, 2486–2489 (1987).
- [4] Joannopoulos, J. D., Johnson, S. G., Winn, J. N. & Meade, R. D. *Photonic Crystals: Molding the Flow of Light, Second Edition* (Princeton University Press, 2008).
- [5] Sigalas, M. & Economou, E. N. Band structure of elastic waves in two dimensional systems. *Solid State Commun.* **86**, 141–143 (1993).
- [6] Shechtman, D., Blech, I., Gratias, D. & Cahn, J. W. Metallic phase with long-range orientational order and no translational symmetry. *Phys. Rev. Lett.* **53**, 1951–1953 (1984).
- [7] Levine, D. & Steinhardt, P. J. Quasicrystals: A new class of ordered structures. *Phys. Rev. Lett.* **53**, 2477–2480 (1984).
- [8] Dubois, J.-M. Properties- and applications of quasicrystals and complex metallic alloys. *Chem. Soc. Rev.* **41**, 6760–6777 (2012).
- [9] Vardeny, Z. V., Nahata, A. & Agrawal, A. Optics of photonic quasicrystals. *Nat. Photonics* **7**, 177–187 (2013).
- [10] Kohmoto, M., Sutherland, B. & Iguchi, K. Localization of optics: Quasiperiodic media. *Phys. Rev. Lett.* **58**, 2436–2438 (1987).
- [11] Edagawa, K. Photonic crystals, amorphous materials, and quasicrystals. *Sci. Technol. Adv. Mater.* **15**, 034805 (2014).
- [12] Rechtsman, M. C., Jeong, H.-C., Chaikin, P. M., Torquato, S. & Steinhardt, P. J. Optimized structures for photonic quasicrystals. *Phys. Rev. Lett.* **101**, 073902 (2008).
- [13] Peach, M. Quasicrystals step out of the shadows. *Mater. Today* **9**, 44–47 (2006).
- [14] Simon, B. Almost periodic Schrödinger operators: A review. *Adv. Appl. Math.* **3**, 463–490 (1982).
- [15] Ostlund, S., Prandit, R., Rand, D., Schnellnhuber, H. J. & Siggia, E. D. One dimensional Schrödinger equation with an almost periodic potential. *Phys. Rev. Lett.* **50**, 1873–1877 (1983).
- [16] Kohmoto, M. & Oono, Y. Cantor spectrum for an almost periodic Schrödinger equation and a dynamical map. *Phys. Lett. A* **102**, 145–148 (1984).
- [17] Golden, K., Goldstein, S. & Lebowitz, J. L. Classical transport in modulated structures. *Phys. Rev. Lett.* **55**, 2629–2632 (1985).
- [18] Golden, K., Goldstein, S. & Lebowitz, J. L. Discontinuous behavior of effective transport coefficients in quasiperiodic media. *J. Stat. Phys.* **58**, 669–684 (1990).
- [19] Bergman, D. J. Exactly solvable microscopic geometries and rigorous bounds for the complex dielectric constant of a two-component composite material. *Phys. Rev. Lett.* **44**, 1285–1287 (1980).
- [20] Milton, G. W. Bounds on the complex dielectric constant of a composite material. *Appl. Phys. Lett.* **37**, 300–302 (1980).
- [21] Golden, K. & Papanicolaou, G. Bounds for effective parameters of heterogeneous media by analytic continuation. *Comm. Math. Phys.* **90**, 473–491 (1983).
- [22] Milton, G. W. *The Theory of Composites*. Cambridge Monographs on Applied and Computational Mathematics (Cambridge University Press, 2002).
- [23] Murphy, N. B., Cherkaev, E., Hohenegger, C. & Golden, K. M. Spectral measure computations for composite materials. *Commun. Math. Sci.* **13**, 825–862 (2015).
- [24] Murphy, N. B., Cherkaev, E. & Golden, K. M. Anderson transition for classical transport in composite materials. *Phys. Rev. Lett.* **118**, 036401 (2017).
- [25] Arakelian, S. et al. Formation of quasiperiodic bimetal thin films with controlled optical and electrical properties. In Andrews, D. L., Nunzi, J.-M. & Ostendorf, A. (eds.) *Nanophotonics VI*, vol. 9884, 509 – 516. International Society for Optics and Photonics (SPIE, 2016).
- [26] Nandhagopal, P., Pal, A. K. & Bharathi Mohan, D. Fabrication of silver and silver-copper bimetal thin films using co-sputtering for SERS applications. *Opt. Mater.* **97**, 109381 (2019).
- [27] Genov, D. A., Sarychev, A. K., Shalaev, V. M. & Wei, A. Resonant field enhancements from metal nanoparticle arrays. *Nano Lett.* **4**, 153 – 158 (2004).
- [28] Genov, D. A., Shalaev, V. M. & Sarychev, A. K. Surface plasmon excitation and correlation-induced localization-delocalization transition in semicontinuous metal films. *Phys. Rev. B* **72**, 113102 (2005).
- [29] Dallapiccola, R., Gopinath, A., Stellacci, F. & Negro, L. D. Quasi-periodic distribution of plasmon modes in two-dimensional Fibonacci arrays of metal nanoparticles. *Opt. Express* **16**, 5544–5555 (2008).
- [30] Shenhar, R. & Rotello, V. Nanoparticles: Scaffolds and building blocks. *Acc. Chem. Res.* **36**, 549–561 (2003).
- [31] Bergman, D. J. & Stroud, D. Physical properties of macroscopically inhomogeneous media. *Phys. Solid State* **46**, 147–269 (1992).
- [32] Clerc, J. P., Giraud, G., Laugier, J. M. & Luck, J. M. The electrical conductivity of binary disordered systems, percolation clusters, fractals, and related models. *Adv. Phys.* **39**, 191–309 (1990).
- [33] Jonckheere, T. & Luck, J. M. Dielectric resonances of binary random networks. *J. Phys. A Math. Theor.* **31**, 3687–3717 (1998).
- [34] Cherkaev, E. Inverse homogenization for evaluation of effective properties of a mixture. *Inverse Probl.* **17**, 1203–1218 (2001).

- [320] Stauffer, D. & Aharony, A. *Introduction to Percolation Theory* (Taylor and Francis, London, 1992), second edn.
- [321] [36] Torquato, S. *Random Heterogeneous Materials: Microstructure and Macroscopic Properties* (Springer-Verlag, New York, 2002).
- [322] [37] Zhang, S. *et al.* Abnormal conductivity in low-angle twisted bilayer graphene. *Sci. Adv.* **6**, eabc5555 (2020).
- [324] [38] Guhr, T., Müller-Groeling, A. & Weidenmüller, H. A. Random-matrix theories in quantum physics: Common concepts. *Phys. Rep.* **299**, 189–425 (1998).
- [326] [39] Canali, C. M. Model for a random-matrix description of the energy-level statistics of disordered systems at the Anderson transition. *Phys. Rev. B* **53**, 3713–3730 (1996).